Interwell intersubband electroluminescence from Si/SiGe quantum cascade emitters

R. Bates, S. A. Lynch, D. J. Paul, Z. Ikonic, R. W. Kelsall, P. Harrison, S. L. Liew, D. J. Norris, A. G. Cullis, W. R. Tribe, and D. D. Arnone

Citation: Applied Physics Letters **83**, 4092 (2003); doi: 10.1063/1.1626003
View online: http://dx.doi.org/10.1063/1.1626003
View Table of Contents: http://scitation.aip.org/content/aip/journal/apl/83/20?ver=pdfcov
Published by the AIP Publishing

jInterwell intersubband electroluminescence from Si/SiGe quantum cascade emitters

R. Bates, S. A. Lynch,[a)] and D. J. Paul
University of Cambridge, Cavendish Laboratory, Madingley Road, Cambridge, CB3 0HE, United Kingdom

Z. Ikonic, R. W. Kelsall, and P. Harrison
University of Leeds, Institute for Microwaves and Photonics, School of Electronic and Electrical Engineering, Leeds, LS2 9JT, United Kingdom

S. L. Liew, D. J. Norris, and A. G. Cullis
University of Sheffield, Department of Electronic and Electrical Engineering, Mappin Street, Sheffield, S1 3JD, United Kingdom

W. R. Tribe and D. D. Arnone
Tera View Limited, 302-304 Cambridge Science Park, Milton Road, Cambridge, CB4 0WG, United Kingdom

(Received 12 May 2003; accepted 17 September 2003)

The quantum cascade laser provides one potential method for the efficient generation of light from indirect materials such as silicon. While to date electroluminescence results from THz Si/SiGe quantum cascade emitters have shown higher output powers than equivalent III–V emitters, the absence of population inversion within these structures has undermined their potential use for the creation of a laser. Electroluminescence results from Si/SiGe quantum cascade emitters are presented demonstrating intersubband emission from heavy to light holes interwell (diagonal) transitions between 1.2 THz (250 μm) and 1.9 THz (156 μm). Theoretical modeling of the transitions suggests the existence of population inversion within the system. © *2003 American Institute of Physics.* [DOI: 10.1063/1.1626003]

There are many potential applications for terahertz radiation but, at present, this part of the electromagnetic spectrum (1 to 10 THz) is underutilized due to the difficulty of realizing cheap practical sources and detectors. These applications include medical and dental imaging,[1] pollution monitoring, pathogen detection,[2] and security screening. Recent developments within III–V quantum cascade lasers have seen operation at 4.4 THz.[3] Operating on an interminiband transition and using a chirped superlattice to allow rapid depopulation of the lower laser levels, pulsed operation has been observed at temperatures up to 80 K.

There are, however, a number of physical reasons why the Si/SiGe materials system may have advantages over III–V technologies at this frequency range. First, the thermal conductivity of Si substrates is approximately three times greater than III–V substrates, thus making it easier to dissipate excess heat. Second, the group IV–IV nature of the SiGe bond means that there is negligible polar optical phonon scattering. The absence of this scattering mechanism results in significantly enhanced intersubband lifetimes, a fact which has been experimentally verified.[4] Intersubband lifetime measurements of modulation-doped SiGe show no reduction in lifetimes up to 100 K, in contrast with GaAs which shows phonon scattering dominating the intersubband lifetimes above 40 K.[5] Other potential benefits of Si include low cost, mature processing techniques, and the possible integration with Si microelectronics.

MIR Si/SiGe cascade emitters have been demonstrated using heavy hole (HH) to HH intersubband transitions.[6] Light hole (LH) to HH intersubband electroluminescence has been demonstrated at THz frequencies both along modulation-doped p-type Si/SiGe quantum wells[7] and within a quantum cascade structure.[8] The quantum cascade emission at THz frequencies was based upon intrawell (vertical) transitions at 2.9 and 8.9 THz (LH1 to HH1 and HH2 to HH1). It is difficult however, to attain the population inversion required to produce a laser in this type of structure. This is because the tunneling rate controlling carrier injection into the upper energy level will be nominally the same as the tunneling rate controlling the depopulation of the lower energy into the next adjacent well. This letter demonstrates far-infrared electroluminescence from interwell, or diagonal, subband transitions within Si/SiGe quantum cascade heterostructures. It is easier to obtain a population inversion in this type of structure since the tunneling rates can now be tuned by altering the electric field across the structure. This type of structure also has the added advantage that the transition energies can be tuned with an applied electric field. Using parameters extracted from materials characterization, the best theoretical fits for the experimental emission spectra suggest that a population inversion is present. In contrast, there is poor agreement between experimental and theoretical spectra if thermal equilibrium populations are used. Spectral measurements also show polarization resolved features which are attributed to interwell subband transitions and agree well with the predicted transition energies. Moreover, the observed shift in transition energy with increasing bias voltage is a signature of an interwell transition.

The wafer used for this work was purchased from Qine-

[a)]Electronic mail: sal44@cam.ac.uk

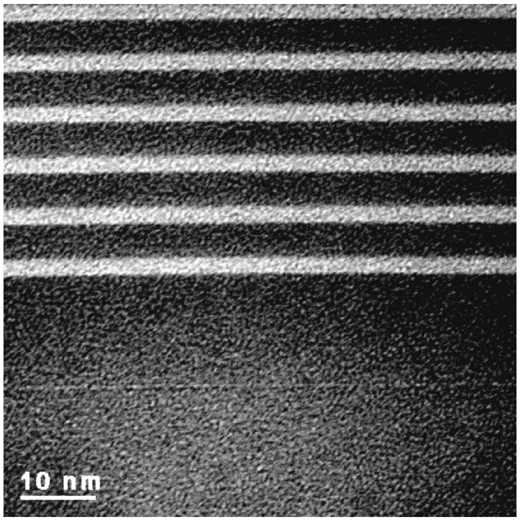

FIG. 1. A transmission electron micrograph showing a few quantum wells and barriers at the bottom (near substrate) of the active cascade part of the wafer with a graded injector below the bottom barrier in the picture.

tiQ, Malvern, U.K., having been grown on a 150 mm p^- Si(100) substrate in an Applied Centura low-pressure chemical vapor deposition system. SiH_4 and GeH_4 were used in a H_2 carrier gas, with p-type doping provided by B_2H_6. Typical growth parameters can be found in Ref. 9. A $\sim 3\ \mu m$ linearly graded $Si_{1-x}Ge_x$ buffer was grown followed by $\sim 1\ \mu m$ $Si_{0.8}Ge_{0.2}$ constant composition to provide a strain relaxed buffer on top of which the strain symmeterized active regions were deposited. The cascade region consisted of a 200 nm p-$Si_{0.8}Ge_{0.2}$ bottom contact ($N_A = 3 \times 10^{20}\ cm^{-3}$), a 15 nm graded injector layer from i-$Si_{0.8}Ge_{0.2}$ to i-$Si_{0.72}Ge_{0.28}$, then 100 periods of 2.2 nm i-Si barriers with 4.4 nm i-$Si_{0.72}Ge_{0.28}$ quantum wells. The cascade was capped with a 2.2 nm i-Si barrier, a 15 nm graded injector, and 40 nm p-$Si_{0.79}Ge_{0.21}$ contact layer $N_A = 5 \times 10^{19}\ cm^{-3}$). The layer thicknesses have been measured by transmission electron microscopy (TEM), Fig. 1, while the Ge contents were obtained from energy dispersive x-rays and energy filtered TEM. These experimentally measured parameters were then used to calculate the band structure of the material as grown.

Samples were etched into $240 \times 240\ \mu m^2$ mesas using $SiCl_4$ reactive ion etching and Al(1%Si) evaporated to form ohmic contacts. A rapid thermal anneal below 420 °C was performed to prevent spiking of the contacts into the active regions. Fourier transform infrared spectroscopy was performed using a Bruker 66V stepscan spectrometer with a liquid-He-cooled Si bolometer for detection. The sample was placed in a continuous flow cryostat providing measurement temperatures between 4.2 and 300 K. Voltage was applied to the sample in the form of a 50 kHz pulse stream with a variable duty cycle. This was gated at 413 Hz to permit measurements using a lock-in amplifier to be performed using the gating pulse as a reference. The bolometer has an optimum frequency response around this frequency. The voltage was applied vertically across the 100 quantum wells, and all parts of the system in which THz radiation propagated were purged with N_2 to eliminate absorption due to water vapor. Three different samples have been measured, and all demonstrate nominally identical properties.

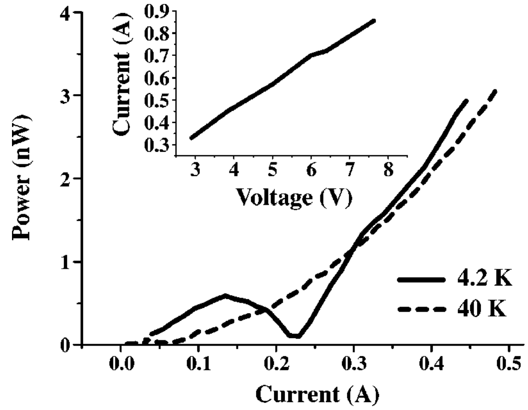

FIG. 2. ($L-V$) characteristics of a typical device for heat sink temperatures of 4.2 K and 40 K with 25% duty cycle. Inset is the $I-V$ characteristics of the device at 4.2 K.

Current–voltage ($I-V$) measurements were performed *in situ* at a heat sink temperature of 4.2 K (insert Fig. 2). Some weak nonlinearities are observed in the $I-V$ characteristic suggesting resonant tunneling of holes. In addition to tunneling between aligned subbands, photon-assisted tunneling is also predicted to occur. Hence, holes may tunnel through the device over a wide range of applied voltages—changing the bias merely changes the ratio of direct and photon-assisted tunnelling. Figure 2 shows a plot of the total integrated power over the spectral range 0 to 80 meV against current [luminance–voltage ($L-I$) curve] at heat sink temperatures of 4.2 and 40 K. The local maximum observed at 4.2 K and a current of 150 mA corresponds to emission from B-impurity states.[7,10] Above 200 mA, the emission from these states is quenched. This may be a result of heating in the device as the current is increased. A quasilinear dependence between current and emitted power is observed at 4.2 K beyond 300 mA suggesting that the emission is predominantly from intersubband transitions rather than Joule heating of the device. In contrast, for heat sink temperatures above 40 K with 25% duty cycle or above, the output power scales nonlinearly as a function of the applied current, indicative of Joule heating. All measurements have therefore been performed at 10% duty cycles or less and at 4.2 K to minimize heating effects.

Figure 3 shows the experimentally measured (solid line)

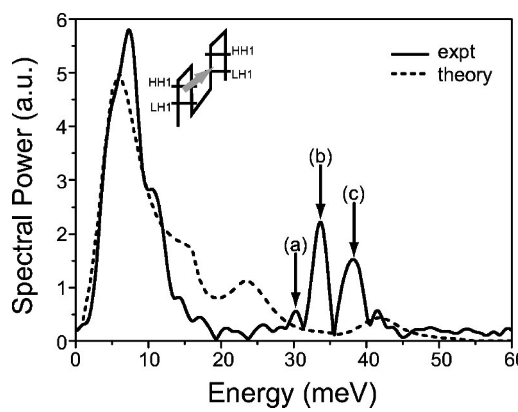

FIG. 3. TE polarized edge emission taken under an applied bias of 6.4 V (10% duty cycle) at 4.2 K (solid line) and theoretical predictions (dashed line).

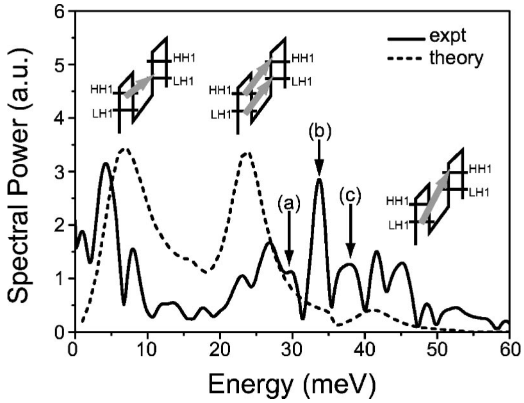

FIG. 4. TM polarized edge emission taken under an applied bias of 6.4 V (10% duty cycle) at 4.2 K (solid line) and theoretical predictions (dashed line).

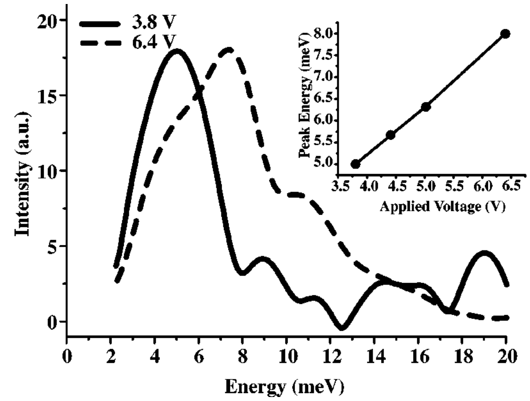

FIG. 5. Evolution of the HH1 to LH1 spectral peak between 3.8 V and 6.4 V with 10% duty cycle at 4.2 K. Note that the magnitude of the two peaks has been scaled to highlight the energy shift. The inset shows the energy of the center of the peak plotted against applied voltage.

and theoretically calculated (dashed line) transverse electric (TE) polarized edge emission spectrum at 4.2 K. The theoretical calculations were performed using a six-band $\mathbf{k}\cdot\mathbf{p}$ model with self-consistent inclusion of the internal charge density. Exact details of these calculations are published elsewhere.[11] The strong feature centered at 8 meV is attributed to the lowest-energy HH1–LH1 interwell transition. Between 30 and 40 meV, three sharp features are observed, labeled (a), (b), and (c). These correspond to the B-impurity state transitions mentioned earlier, and can be identified as, (a) $1s-2p^1$ (30.4 meV), (b) $1s-2p^2$ (34.5 meV), and (c) $1s-2p^4$ (39.6 meV).[10] It should be noted that at small bias currents, these B-impurity state transitions are the only features observed in the emission spectrum. It is these features which account for the local maximum in the $L-I$ curve in Fig. 2 between 0 and 200 mA. From this graph, it is clear that there is good agreement between the observed and predicted transition energy of the HH1–LH1 transition. The situation is considerably different for the transverse magnetic (TM) polarized emission in Fig. 4. This spectrum is very complicated and contains addition features. First, the B-impurity states, labeled (a), (b), and (c), are again visible as expected in the 30–40 meV energy range. There is an additional sharp peak at 8 meV which is almost certainly due to a B-impurity transition. The transition energy of this feature agrees very well with the strong emission observed recently in B-doped Si.[12] Unfortunately, the presence of these impurity transitions makes it difficult to clearly resolve the weaker underlying intersubband transitions in this polarization. The broad feature between 20 and 30 meV, is identified as the degenerate LH1–LH1 and HH1–HH1 interwell transitions. Another weak feature between 50 and 60 meV, also not visible in the TE polarization, lies close to the predicted higher-energy interwell LH1–HH1 transition. In Fig. 5, the low-energy part of the spectrum highlighting the transition of greatest interest is blown up. Figure 5 shows the evolution of the HH1–LH1 transition energy as the bias voltage is increased from 3.8 V to 6.4 V. The relative magnitude of the peaks here are not the same but have been scaled to highlight the energy shift. Also shown in the inset is a graph of transition energy against bias voltage. It is this clear shift in transition energy which provides the evidence for an interwell subband transition. Intrawell subband transitions are expected to remain fixed at the subband separation energy.

In conclusion, a 100 period SiGe quantum cascade heterostructure has been grown, and using parameters extracted from materials characterization, theoretical calculations suggest that the structure as grown should exhibit population inversion. Spectral measurements show polarization resolved features which are attributed to interwell subband transitions, and which agree well with the predicted transition energies. Moreover, the observed shift in transition energy with increasing bias voltage provides strong evidence that the observed transitions are interwell. This positive result supports the case that the Si/SiGe materials system does indeed have the potential for the realization of a quantum cascade laser.

This work was funded by U.S. DARPA under Air Force Contract No. F-19628-99-C-0074. The authors would like to thank David Robbins, Richard Soref, and Edgar Martinez for useful discussions and support.

[1] D. D. Arnone, C. M. Ciesla, and M. Pepper, Phys. World **13**, 35 (2000).
[2] X.-M. Wang, Q. Chen, J.-M. Ruysschaert, and V. Cabiaux, Biochemistry **35**, 14939 (1996).
[3] R. Köhler, A. Tredicucci, F. Beltram, H. E. Beere, E. H. Linfield, A. G. Davies, D. A. Ritchie, and R. C. Iotta, Nature (London) **417**, 156 (2002).
[4] C. R. Pidgeon, P. Murzyn, J.-P. R. Wells, I. V. Bradley, Z. Ikonic, R. W. Kelsall, P. Harrison, S. A. Lynch, D. J. Paul, D. D. Arnone, D. J. Robbins, D. J. Norris, and A. G. Cullis, Appl. Phys. Lett. **80**, 1456 (2002).
[5] G. Sun, L. Friedman, and R. A. Soref, Appl. Phys. Lett. **66**, 3425 (1995).
[6] G. Dehlinger, L. Diehl, U. Gennser, H. Sigg, J. Faist, K. Ensslin, D. Grützmacher, and E. Müller, Science **290**, 2277 (2000).
[7] D. J. Paul, S. A. Lynch, R. Bates, Z. Ikonic, R. W. Kelsall, P. Harrison, D. J. Norris, S. L. Liew, A. G. Cullis, D. D. Arnone, C. R. Pidgeon, P. Murzyn, J.-P. R. Wells, and I. V. Bradley, Physica E (Amsterdam) **16**, 147 (2003).
[8] S. A. Lynch, R. Bates, D. J. Paul, D. J. Norris, A. G. Cullis, Z. Ikonic, R. W. Kelsall, P. Harrison, D. D. Arnone, and C. R. Pidgeon, Appl. Phys. Lett. **81**, 1543 (2002).
[9] D. J. Paul, A. Ahmed, N. Griffin, M. Pepper, A. C. Churchill, D. J. Robbins, and D. J. Wallis, Thin Solid Films **321**, 181 (1998).
[10] C. Jagannath, Z. W. Grabowski, and A. K. Ramdas, Phys. Rev. B **23**, 2082 (1981).
[11] Z. Ikonic, P. Harrison, and R. W. Kelsall, Phys. Rev. B **64**, 245311 (2001).
[12] I. V. Altukhov, E. G. Chirkova, V. P. Sinis, M. S. Kagan, Y. P. Gousev, S. G. Thomas, K. L. Wang, M. A. Odnoblyudov, and I. N. Yassievich, Appl. Phys. Lett. **79**, 3909 (2001).